Int. J. Electrochem. Sci., 9 **(2014)** 6765 - 6780

International Journal of
ELECTROCHEMICAL
SCIENCE
www.electrochemsci.org

Investigations on the Corrosion-Enhanced Erosion Behavior of Carbon Steel AISI 1020

J. Malik, I.H. Toor[*] *, W.H. Ahmed, Z.M. Gasem, M.A. Habib, R. Ben-Mansour and H.M. Badr*

Dept. of Mechanical Engineering, King Fahd University of Petroleum & Minerals (KFUPM)
Dhahran 31261, Kingdom of Saudi Arabia
[*]E-mail: ihsan@kfupm.edu.sa, ihsan_jut@hotmail.com

Received: 25 May 2014 / *Accepted:* 4 August 2014 / *Published:* 29 September 2014

In this study, corrosion-enhanced erosion behavior of AISI 1020 carbon steel was examined. The specimens were subjected to immersion test in ferric chloride solution (100 g $FeCl_3$ in 900 ml of distilled water), and subsequently followed by solid particle erosion experiments. In order to simulate the corrosion behavior and subsequent erosion, different immersion times were selected, i.e. 12 h, 24 h, 36 h, 48 h and 60 h. After the immersion tests, corrosion rates were calculated for each time based on weight loss measurements. Later the corroded specimens were subjected to solid particle erosion (SPE) investigations. Angular alumina with 50 µm particle size was used as an erodent in SPE experiments. Significant increase in erosion rates of corroded carbon steel 1020 samples was observed which is attributed to hard and brittle corrosion products that are formed on the surface after corrosion. Erosion rate for 24 h immersed specimens was the highest compared to all other specimens. This was attributed to the maximum hardness and surface roughness of the 24 h immersed specimens. Detailed scanning electron microscopy (SEM) investigations were carried out on as received, corroded and eroded specimens, in order to evaluate the material degradation behavior in corrosion enhanced erosion process. X-ray diffraction spectroscopy (XRD) was also carried out on corroded specimens to identify the scales formed during immersion experiments.

Keywords: Corrosion enhanced erosion; Immersion; Erosion rate; AISI 1020 carbon steel,

1. INTRODUCTION

In many industrial applications, the stagnant solutions that remains in the pipelines can make these pipelines susceptible to corrosion. During the operations, solid particles entrained in the fluid can further aggravate mass loss at the corrosion sites and this phenomenon is known as corrosion-enhanced erosion. Solid particle erosion is a mechanical degradation process in which the material gradually

wears away through subsequent impact by abrasive particles. While erosion-corrosion involves mechanical wear by solid particles in conjunction with electrochemical dissolution by the corrosive solution, with both activities occurring simultaneously in a dynamic two-phase flow system [1]. The underlying mechanism in erosion-corrosion depends on whether erosion precedes corrosion and/or corrosion precedes erosion, and the latter is known as corrosion-enhanced erosion. Matsumura [2] explains the effect of corrosion on erosion and attributes the enhancement of erosion to the removal of work hardened layer which is caused or accelerated by corrosion attack. Other mechanisms include: i) selective corrosion attack at grain boundaries resulting in increased susceptibility of grain removal by erosion [3], and ii) increase in the number of surface defects due to micro-pitting [4].

Previously, many researchers have investigated the erosion-corrosion behavior of steels using various systems, such as rotating electrode systems [5-8], flow loop systems 9-13] and jet impingement systems [14-18]. Islam et al. [19] recently studied the erosion-corrosion behavior of API X-70 steel by carrying out cyclic erosion and corrosion tests on the steel surface and hence, determined the erosion-enhanced corrosion and corrosion-enhanced erosion of their test specimen. It was found that the corrosion attack removes the work hardened layer and exposes stress-free surface to the erosion as a result the erosion of corroded surface is greatly enhanced. Dong et al. [20] investigated the erosion-accelerated corrosion of a carbon steel 1020 and stainless steel 316L in a galvanic couple. The results indicated that as the flow velocity increases, erosion becomes a dominating variable in the synergism of the galvanic couple. Hence, the pure erosion and corrosion-enhanced erosion components dominated the overall erosion-corrosion process.

Mechanical and electrochemical interactions during the erosion-corrosion of carbon steel A1045 were reported by Guo et al. [7]. The corrosion-enhanced erosion increased with an increase in anodic current density due to corrosion induced damage in the surface layer of the alloys. In contrast, Neville et al. [21] in their study of erosion-corrosion behavior of high-alloy stainless steels highlighted that resistance to weight loss does not increase with an increase in the hardness. Nava et al. [22] investigated the effect of hardness on erosion-corrosion resistance of various materials and they concluded that the erosion-corrosion damage increases with increasing hardness at high temperatures. The increase in erosion corrosion was attributed to the non-adherent and less protective oxide scale formation.

In the present study, a different approach is used to study the corrosion-enhanced erosion behavior of carbon steel AISI 1020. The test specimens were corroded by immersing in low pH and high chloride environments. The corroded specimens were then subjected to solid particle erosion, to simulate the corrosion enhanced erosion behavior and results were compared with that of non-corroded specimens. Furthermore, the corrosion-enhanced erosion behavior is correlated with the material hardness and surface roughness. Finally, the metallurgical investigations were carried out using XRD and SEM in order to identify the corrosion products and evaluate the material degradation mechanism involved in corrosion enhanced erosion process.

2. EXPERIMENTAL DETAILS

Table 1. Chemical composition of carbon steel AISI 1020

Alloy	Fe	C	Si	Mn	Cr	Ni	Mo	Co	Cu	P	S
AISI 1020	98.7	0.21	0.14	0.78	0.03	0.03	…	0.01	0.02	0.02	0.012

Table 1 shows the chemical composition of the test material (AISI 1020) used in this study. This alloy is extensively used in variety of industrial applications where it undergoes erosion-corrosion and corrosion enhanced erosion problems such as oil & gas pipelines, valves and gas turbine systems. Carbon steel AISI 1020 was immersed in ferric chloride solution (100 g $FeCl_3$ in 900 ml of distilled water) at set temperature of 25° C. Immersion tests were carried out for different times (12 h, 24 h, 36 h, 42 h and 60 h) and the weight loss was measured. Before the tests, specimens of size 25 mm x 25 mm x 5 mm were cold mounted in epoxy, to expose only the specimen surface to the corrosive solution and to avoid any crevice corrosion at the edges which could influence the weight loss readings. . The exposed surface area after mounting was 625 mm^2 (25 x 25 mm). After mounting, specimens were ground up to 400 grit size on SiC abrasive paper, cleaned with distilled water, dried, and weighed to an accuracy of 0.0001 g. A reference epoxy sample (without test specimen) of similar size as of other mounts was also immersed in the solution to analyze and eliminate any error in weight loss due to epoxy mounts.). After immersion, corroded specimens were carefully rinsed with distilled water, air-dried, and the weight loss was measured. The weight loss method is in accordance with the ASTM G 31-72 immersion test standard [23]. The corrosion rate (CR) was calculated based on the weight loss method using the following equation [24]:

$$CR = \left| \frac{weight\ loss\ (g)}{surface\ area\ (mm^2) \times density\ (g/mm^3) \times time\ (h)} \right| \times 8760\ yr^{-1} \qquad (1)$$

Where, surface area of 625 mm^3 and the theoretical density of $7.87x10^{-3}$ g/mm^3 for carbon steel AISI 1020, was used in the CR calculations.

CSM Micro Combi Tester was employed to measure the hardness of corroded surfaces of carbon steels AISI 1020 specimens. Corroded samples were cut using a low velocity, diamond blade precision cutter to avoid any tempering of the surface while cutting. Samples were then mounted such that the hardness profiles of cross-section could be recorded. Low load of 20 mN was selected to measure the hardness of corrosion products. A total of 6 readings were taken on each specimen and hence, their average value was calculated (Table 2). Surface roughness on corroded and polished specimens was measured using Starret Roughness Tester (Model SR200). Eight readings were measured on each set of specimens and hence, the average surface roughness Ra (µm) is reported.

Table 2. Microhardness of the test materials

Immersion Time (h)	Vickers Hardness					Average
0	240.95	233.83	236.69	235.45	237.39	236.86
12	274.62	364.74	292.17	282.81	336.89	310.25
24	279.06	362.44	346.02	355.59	328.18	334.26
36	286.22	258.08	260.33	211.40	276.05	258.42
48	268.89	246.31	261.85	239.74	256.11	254.58
60	226.93	311.96	269.40	250.40	308.29	273.40

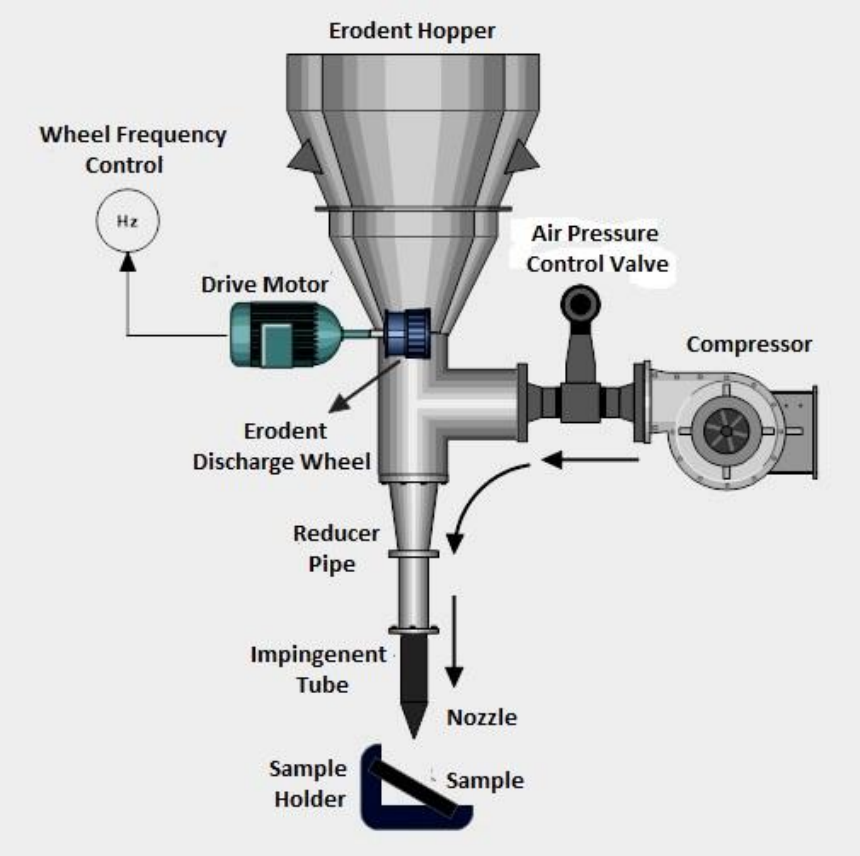

Figure 1. Schematic of air jet erosion tester (not drawn to scale)

For erosion experiments on corroded surfaces, Air Jet Erosion Tester manufactured by KOEHLER Instrument Company, Inc. (Model # K93700) was utilized, as shown in Fig. 1. Erosion tests were performed as per ASTM G-76-95 test standard [25]. Particle flow rate (g/min) was precisely controlled by the rotation frequency of the discharge wheel, located at the outlet of the erodent hopper. Particle flow rate was calculated by collecting and measuring the erodent mass flowing through the nozzle for 10 min at a specified wheel frequency. Impact velocity was measured with an accuracy of ± 2m/s, using double disc rotating method, described elsewhere [26]. Both particle flow rate and impact

velocity calibrations were checked after every 20 experiments. Angular shape alumina erodent with particle size of 50 μm was used in all the erosion experiments.

Erosion tests were carried out on corroded (24 h immersed, and 48 h immersed specimens,) as well as un-corroded specimens at two different velocities: 30 and 60 m/s. At each impact velocity six different impact angles were used: 15°, 30°, 45°, 60°, 75°, and 90°. In addition, erosion tests at single set of parameters (i.e., impact velocity = 60 m/s and angle = 90°) was carried out for 0 h, 12 h, 24 h, 36 h, 48 h and 60 h immersed specimens. This was done to analyze the effect of immersion time on erosion rates of these specimens. Particle flow rate of 2.5 g/min was used in all the erosion tests, which was selected to allow adequate particle flux on the specimen yet avoiding high inter-particle collisions which are caused by using high particle flow rates [27-28]. Specimens subjected to erosion testing were removed after every 2 min, cleaned and reweighed, repeated for a total time of 10-15 min. Hence, mass loss against the erodent mass was plotted and steady state erosion rate was calculated from the slope of the mass loss versus erodent mass graph.

Scanning electron microscopy (SEM) was employed to analyze the surface degradation after pure erosion, pure corrosion, and corrosion enhanced erosion of carbon steel AISI 1020. Furthermore, X-Ray diffraction (XRD) was used to characterize the corrosion products formed on the specimens after immersion. XRD measurements were carried out on a Bruker D8 Advance diffractometer, using Cu(Kα) source. The scans were obtained in the range of 5-80° (2θ). The XRD patterns of the corroded specimens were obtained from the rust which was scraped and collected from the corroded specimens.

3. RESULTS & DISCUSSION

3.1. Corrosion investigations using immersion test

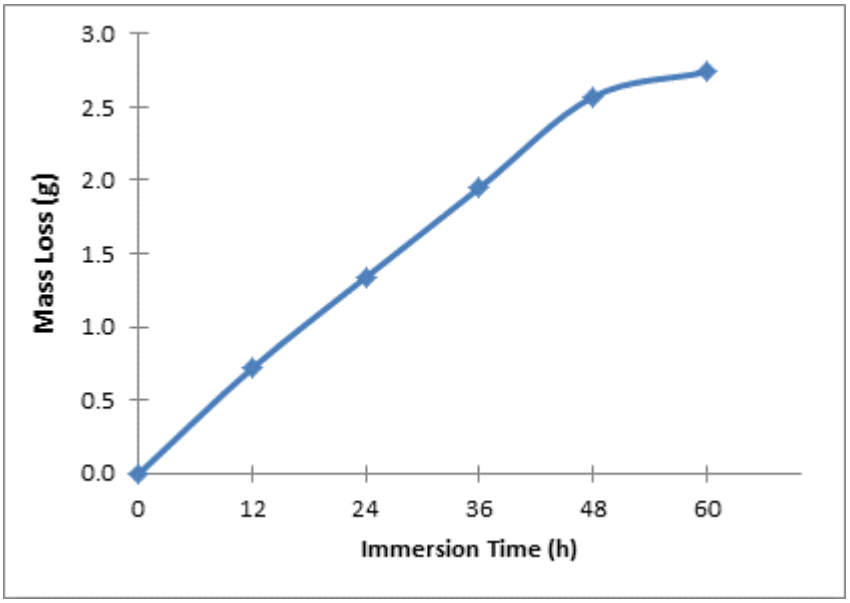

A

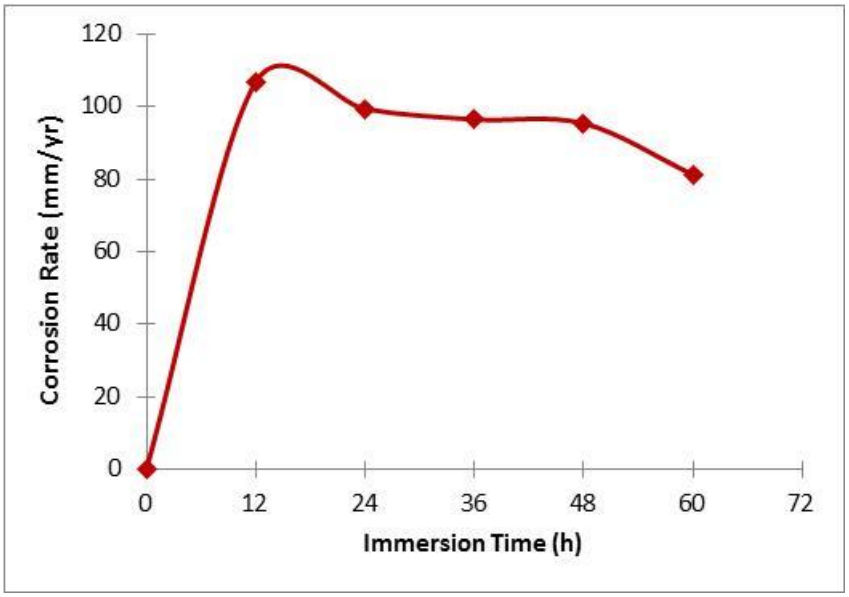

B

Figure 2. (a) AISI 1020 mass loss (g) at different immersion times (h) and (b) Corrosion rate (mm/yr) of AISI 1020 versus immersion time (h) [24].

Carbon steel used in this investigation has a typical microstructure, comprising of pearlite colonies in a ferrite matrix. Weight loss (g) and corrosion rate (mm/yr) values for carbon steel AISI 1020 after immersion tests at different times are presented in Table 3. The corrosion rate (CR) was calculated based on Eq. 1 mentioned above [24]:

Figs. 2 (a) and (b) graphically represents the variation in mass loss and corrosion rate, respectively. It can be seen from Fig. 2(a), that the weight loss of carbon steel gradually increases with immersion time. An average weight loss of 0.72 g was recorded after 12 h of immersion, which increased by almost 4 times to 2.47g after 60 h of immersion. Garcia et al. [29] studied the adherent and non-adherent rust formation on carbon steel AISI 1020 after immersion in chloride solution and found that the weight of non-adherent rust that is lost during the corrosion process, decreased with time, consequently, a more adherent rust is formed. Hence, the increase in weight loss for AISI 1020 with immersion time can be attributed to the loss of non-adherent layer of rust during immersion.

Table 3. Mass loss (g) and corrosion rate (mm/yr) for carbon steel AISI 1020 immersed at different times.

Immersion Time (h)	0	12	24	36	48	60
Mass Loss (g)	0	0.72	1.34	1.95	2.57	2.74
Density (g/mm^3)	7.87×10^{-3}	7.87×10^{-3}	7.87×10^{-3}	7.87×10^{-3}	7.87×10^{-3}	7.87×10^{-3}
Exposed Area (mm^2)	625	625	625	625	625	625
Corrosion Rate (mm/yr)	0	106.8	99.4	96.5	95.4	81.3

However, the instantaneous corrosion rate (mm/yr) shown in Fig. 2(b), is maximum at 12 h and then decreases at higher immersion times. The initial increase in corrosion rate is mainly due to aggressive corrosion attack on bare metal surface. However, as the reaction proceeds and corrosion products starts to form on the metal surface, the ionic activity on the surface is hindered and suppressed, as explained previously by Hu et al. [30].

SEM of the corroded surfaces revealed severe surface degradation due to active corrosion attack by chloride ions (Fig. 3). Ferritic and pearlitic structure can be seen from SEM micrographs of polished specimen (0 h), while the corroded specimens are characterized by formation of troughs (12 h), steps and exfoliated grains (24 h, 36 h and 48), and cracks (60 h). These morphologies were observed in all the corroded specimens irrespective of the immersion time. This indicates continuous formation of brittle corrosion products (cracked regions) and subsequent shredding of the loosely adherent corrosion products leaving behind step-like morphologies.

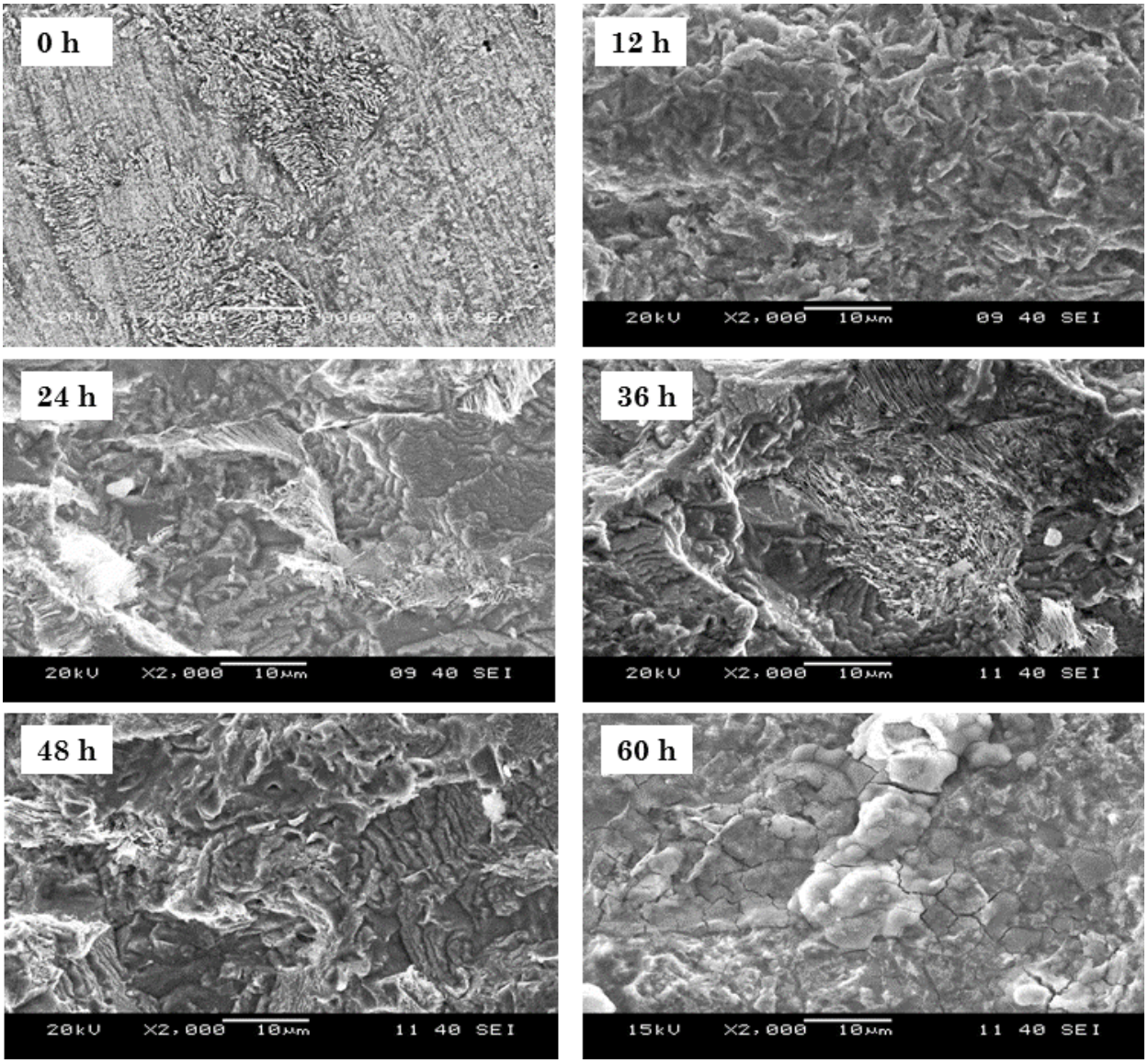

Figure 3. (a) SEM micrograph of polished (0 h) and corroded (12 h, 24 h, 36 h, 48 h, and 60 h) carbon steel AISI 1020.

3.2. Corrosion enhanced erosion using Air Jet impingement

Corroded specimens were subjected to solid particle erosion, thus the enhancement in erosion rate due corrosion was analyzed by comparing the corrosion enhanced erosion rates against pure erosion rates (erosion tests on polished specimens). For 24 h and 48 h immersed specimens, the erosion tests were carried out at impact velocity of 30 m/s and 60 m/s. At each impact velocity, six impact angles from 15° to 90° were used.

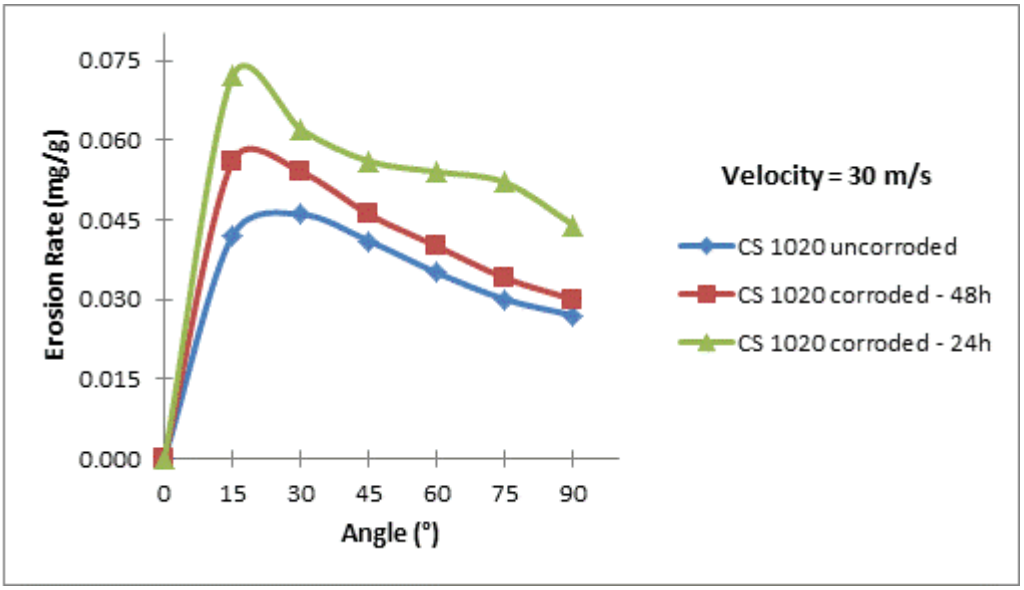

A

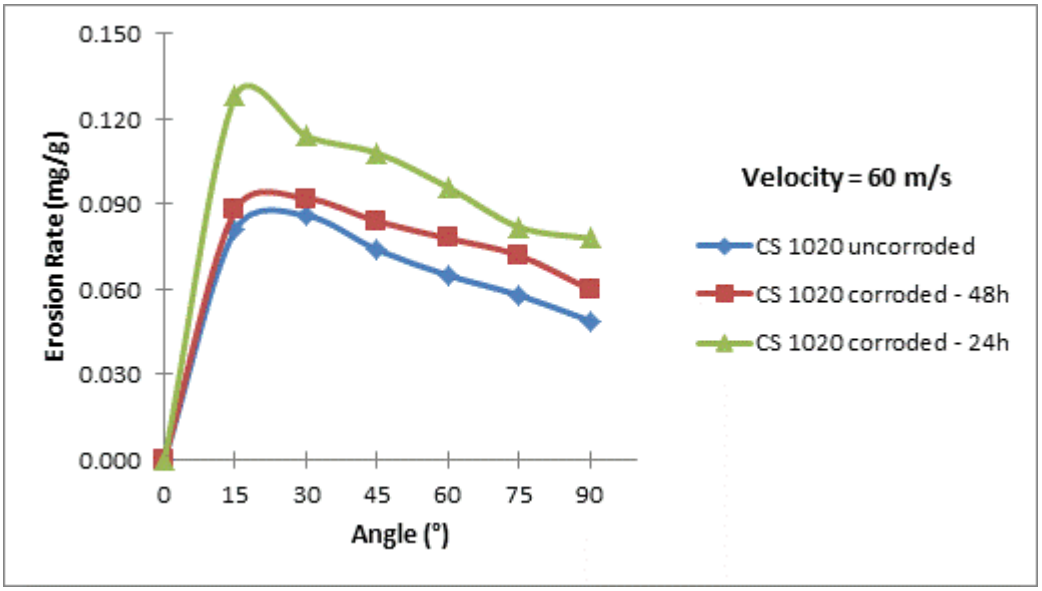

B

Figure 4. Corrosion enhanced erosion and pure erosion comparison of carbon steel AISI 1020 at impact velocity of (a) 30 m/s and (b) 60 m/s.

Fig. 4 (a) and (b) shows the comparison between pure erosion and corrosion enhanced erosion of carbon steel AISI 1020 at impact velocity of 30 m/s and 60 m/s, respectively. Substantial increase in erosion rates for the corroded carbon steel AISI 1020 is observed. Unexpectedly, at both velocities, maximum erosion rate was observed for specimen immersed for 24 h whereas the erosion rate for 48 h immersed specimens was found to be in between polished and 24 h immersed specimens.

This phenomenon was contradicting the expectation of increased erosion rate with an increase in immersion time. Therefore, erosion tests at single set of parameter (impact velocity = 60 m/s and impact angle = 90°) were carried out on specimens immersed for different times (i.e., 0 h, 12 h, 24 h, 36 h, and 48 h) to investigate the variation in erosion rates with immersion time. Fig. 5 shows the result of erosion tests carried on these immersed specimens. It is evident from the figure that the erosion rate varies with immersion time. Nevertheless, the specimen immersed for 24h persistently showed highest erosion rate as compared to other corroded specimens. However, a direct relationship between the effect of immersion time and subsequent enhancement in erosion rate cannot be established for the given data at this stage, because erosion rate is more dependent on material properties such as hardness [31], ductility [32], strength and surface roughness. While the time of immersion mainly results in mass loss which correlates to corrosion rate but in most cases the surface conditions (hardness and surface roughness after corrosion) also varies considerably with immersion time and should not be overlooked. Hence, to correlate the erosion rate with the surface conditions, two important parameters Vickers hardness and surface roughness of the corroded specimens were measured.

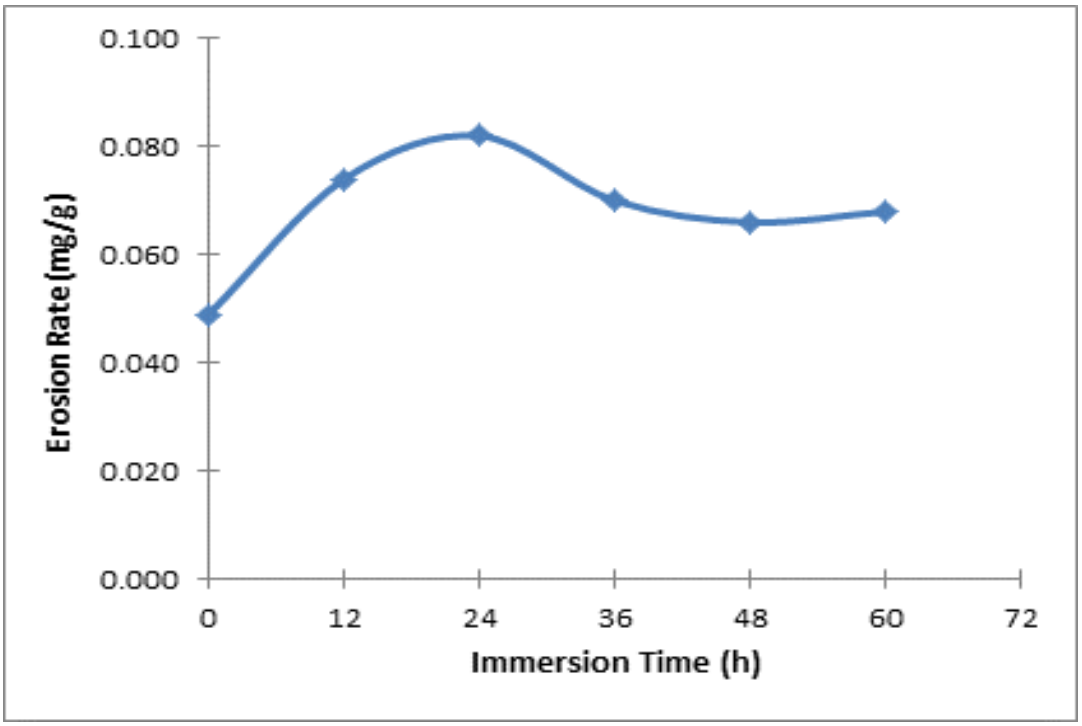

Figure 5. Variation in erosion rates (mg/g) of AISI 1020 at different immersion times (0, 12, 24, 36, 48 and 60 h) at an impact angle of 90°.

Table 4. Vickers hardness and surface roughness values for specimens immersed for different times.

Immersion Time (h)	**0**	**12**	**24**	**36**	**48**	**60**
Hardness (HV)	236.86	310.25	334.26	258.42	254.58	273.40
Roughness (Ra, µm)	0.30	8.77	9.60	8.08	7.79	8.23

Table 4 reveals the average values of Vickers hardness (HV) and surface roughness (Ra, µm) measured on corroded and polished specimens. There is a drastic increase in surface roughness of AISI 1020 from 0.30 µm (polished surface) to a maximum of 9.60 µm (24 h immersed specimen). Surface degradation in carbon steel is mainly due to its inability to form a protective adherent passive layer [33]. Consequently, a combination of adherent and non-adherent rust is formed which contributes to the surface roughness. Variation in hardness can also be seen in Table 4. Increase in hardness was observed for all specimens after immersion tests which may be attributed to brittle corrosion products formed on the surface after corrosion. Hence, the increase in surface roughness and hardness due to the formation of asperities and loosely adhered brittle corrosion products are the main factors which are contributing to the increase in erosion rate of AISI 1020 after the corrosion. Furthermore, an overlay of hardness and erosion rates for corroded specimens is given in the double axis graph shown in Fig. 6a. Surprisingly, the variation in erosion rate directly corresponds to the surface hardness of the corroded specimens. The increase in erosion rate with hardness relates to the inability of harder surface to absorb the kinetic energy of the impacting solid particles [34]. A similar conclusion was reached in our previous work where aluminum 6060 T4-tempered alloy having lower hardness compared to steels, exhibited higher erosion resistance [35].

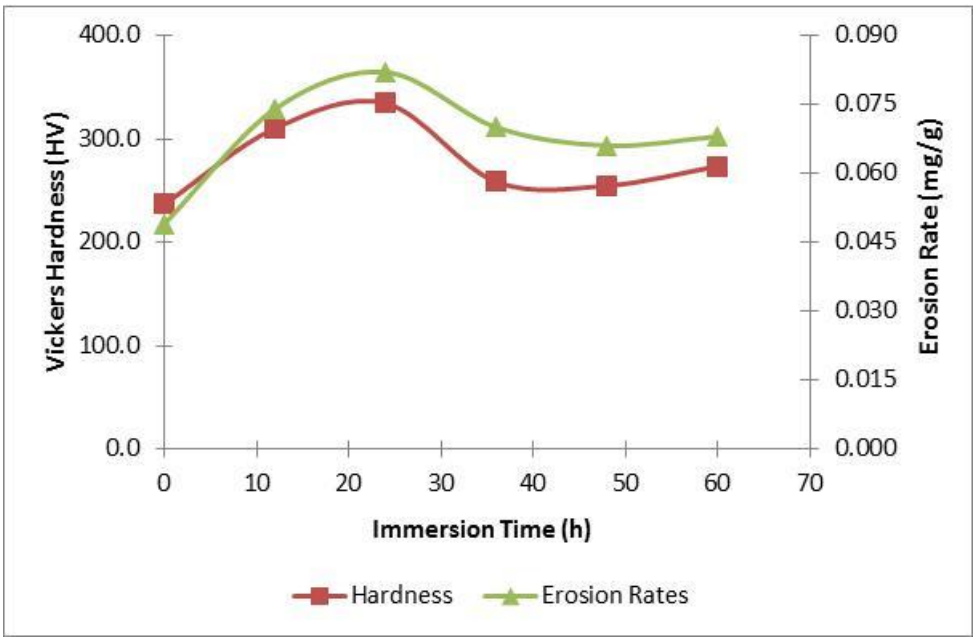

A

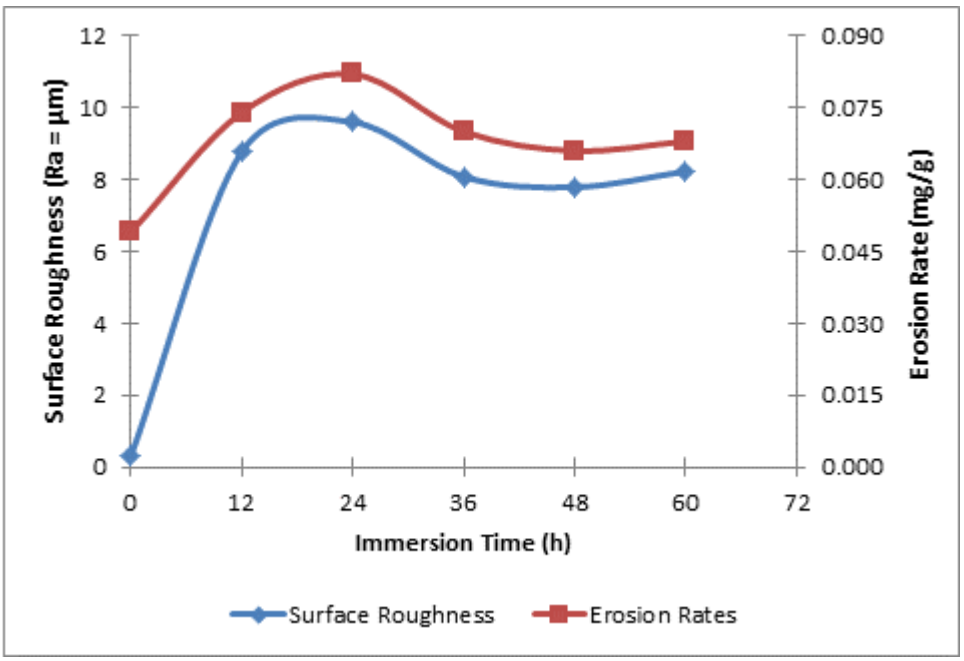

B

Figure 6. (a) Vickers hardness and (b) surface roughness values overlay with erosion rate (impact velocity = 60 m/s and impact angle = 90°) for AISI 1020 specimens immersed at different immersion times (0, 12, 24, 36, 48 and 60 h).

Similarly, the measured surface roughness (Ra, µm) values and erosion rates were superimposed. Fig. 6b clearly shows the variation of erosion rates with surface roughness in a similar fashion as the Vickers hardness. Surface roughness of the target materials plays a vital role and can affect the erosion process of the target material [36].Both, surface roughness and hardness contributed to the variation in the erosion rates. However, it cannot be quantitatively established that which of the two parameters has strongly influenced the erosion rates as both parameters were affected simultaneously during the corrosion process.

3.3. Effect of impact velocity and impact angle on the erosion rate of AISI 1020 carbon steel

The increase in erosion rate with an increase in impact velocity is as expected. From 30m/s to 60 m/s, the erosion rate of AISI 1020 immersed for 24 h, increased from 0.072 mg/g to 0.128 mg/g at an impact angle of 15°. This is due to the increase in particle kinetic energy with increase in impact velocity resulting in higher shear stresses which in turn causes more mass loss [37]. Furthermore, it can be seen that the erosion behavior with respect to impact angle is independent of the impact velocity, similar observation has been reported by other authors previously [38-39]. Ductile and brittle materials exhibit different erosion rates with respect to impact angle. Finnie et al. [40] observed that ductile materials generally show maximum erosion rates in the range of 15°-30° impact angle while brittle materials show maximum erosion rate at normal angle. Similarly, Oka et al. [38] in their erosion rate study of various metals, a plastic and a ceramic showed that the shape of the erosion curves with respect to impact angle depends on material hardness. In addition, the maximum erosion rate at any

given angle was associated with high shear forces incurred on the surface and the ability of the material to resist them. Consequently, materials with high hardness such as ceramics resist material removal at oblique angles while metals being more ductile are prone to shear forces therefore erodes more at oblique angles compared to 90° angle.

Furthermore, Shewmon et al. [41] explained that the high mass loss for ductile metals at oblique angles is due to lip formation by effective penetration of the incident particles. These extruded lips are then sheared off by subsequent impacts whereas at normal incident angle the ductile metals absorb most of the kinetic energy of incoming particles resulting in lower mass loss. Fig. 4 (a) and (b) also shows the effect of impact angle on the erosion rate for carbon steel AISI 1020. It is clear from the figures that the maximum erosion rates occur between 15°-30° impact angle. Accordingly, both corroded and polished specimens are showing ductile erosion behavior.

It is clear from the erosion rate dependence on impact angle that all four materials are following ductile erosion behavior. To understand this ductile erosion mechanism, SEM was carried out, as shown in. Fig. 7 (a) and (b). Fig. 7 shows that the eroded surfaces of carbon steel AISI 1020 at impact velocity of 60 m/s, again, at the impact angle of 15° more wear damage is observed compared to 90°. Deformation scratches and lip formation due to plastic deformation by extrustion/ploughing action can be seen, which is consistent with the findings of other authors [32, 41-42]. At 90° impact angle, the ductile erosion behavior in carbon steel AISI 1020 is characterized by dimples, pits and crater morphologies (Fig. 7 b) which is generally observed in ductile metals at normal impacts [43].

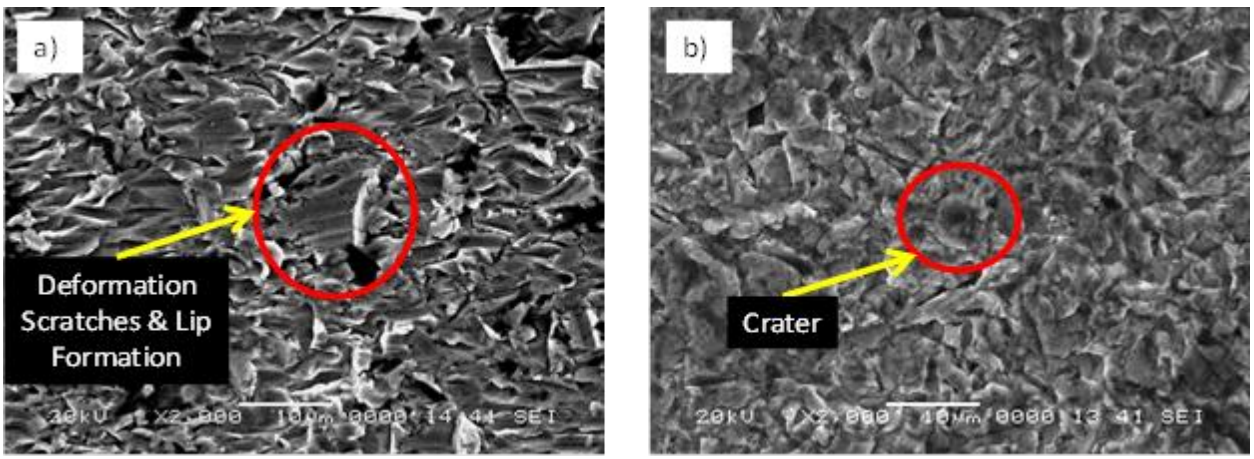

Figure 7. (a) Carbon Steel AISI 1020 eroded surface at impact angle a) 15° and b) 90°

3.4. Corrosion enhanced erosion mechanism

X-Ray diffraction scans were carried out on carbon steel AISI 1020 (24 h and 48 h immersed specimens) in order to characterize the corrosion products and explain the possible reason for the increase in hardness and surface roughness. Fig. 8 compares the XRD patterns of the polished, 24 h corroded and 48 h corroded carbon steel AISI 1020 specimens. The XRD patterns of the corroded samples were obtained from the rust which was scraped and collected from the corroded specimens.

The fittings of the patterns were adequately done using the following components: pure Fe (F), magnetite (M), hematite (H) and another possible compound barringerite (B). The relative decrease in intensity of the F peaks is visible from the patterns.

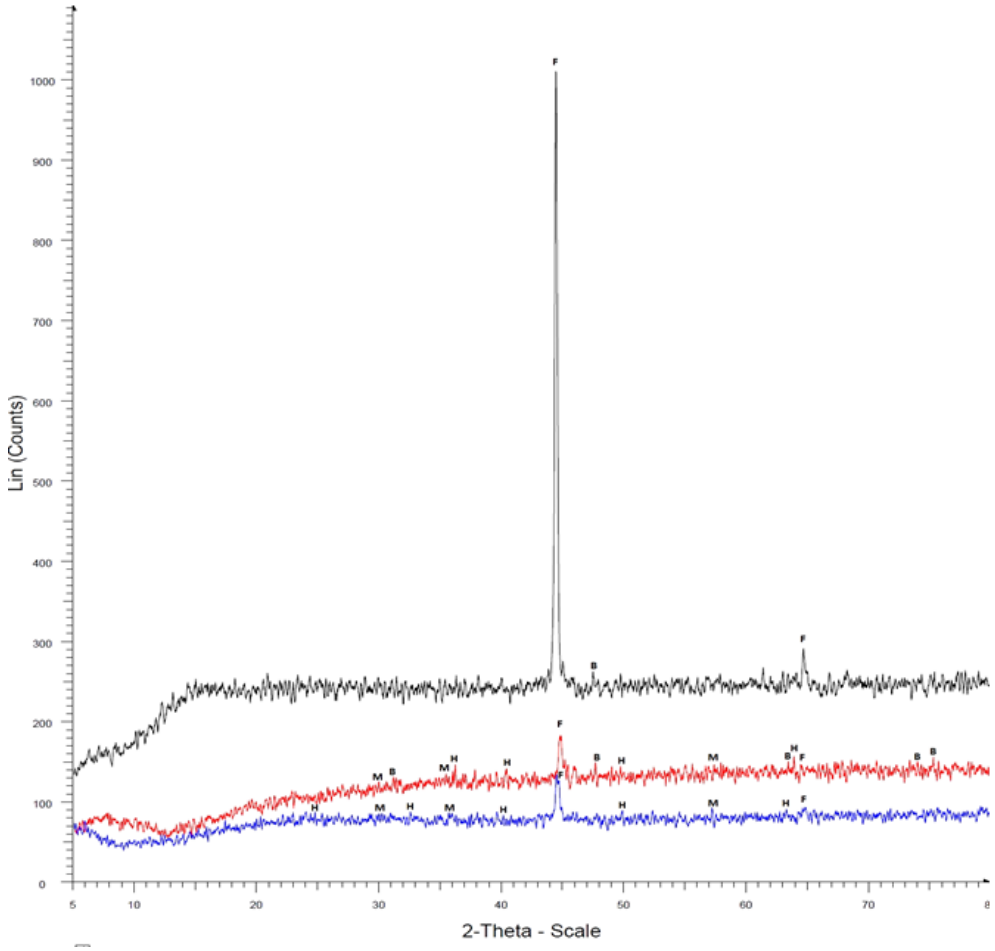

Figure 8. (a) XRD patterns of polished (top curve), 24h corroded (middle curve) and 48h corroded (bottom curve). Peaks labeling: magnetite (M), hematite (H), barringerite (B) and iron (F).

This indicates the conversion of into oxides and other compounds after the immersion tests. Presence of M and H compounds is clearly marked on the XRD patterns of both the corroded specimens. The new peaks of rather lower intensity (abundances) in the patterns of corroded specimens are mostly characteristic of magnetite and hematite phases. Hence, the increase in the surface hardness after corrosion may be attributed to the presence of these brittle phases. In addition, another compound barringerite (Fe_2P) was seen to be in good fit with various peaks of the 24 h corroded specimen. Barringerite is brittle in nature with fine grain size and could be another reason behind the increase in hardness and subsequent erosion rate of the 24 h immersed specimens.

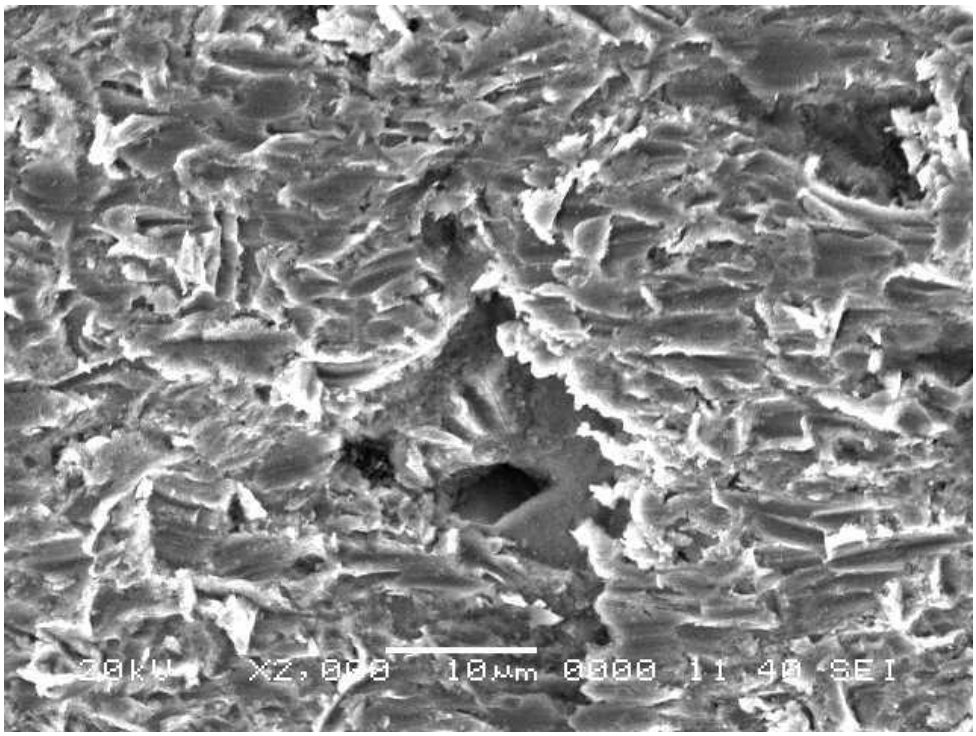

Figure 9. Carbon steel AISI 1020 - 24 h immersed specimen, eroded-corroded surface at impact angle of 15° and velocity of 60 m/s.

Formation of brittle oxide products on AISI 1020 after immersion test is also evident from Fig. 3. Scanning electron microscopy of erosion scars on corroded specimens was carried out to study the corrosion-enhanced erosion mechanism in AISI 1020. Fig. 9 reveals severe surface degradation on 24 h immersed carbon steel surface exposed to erosion test at an impact angle of 15° and impact velocity of 60 m/s. Evidence of heavy plastic deformation by extrusion and forging is clearly visible. Moreover, material cutting, shredding and localized fractures are also dominant during corrosion enhanced erosion of AISI 1020. Extruded lip morphologies, which were observed in pure erosion of AISI 1020, are replaced with fracture induced flattened platelets on corrosion enhanced eroded surface; similar observation was made Islam et al. [19] in their study of corrosion enhanced erosion of API X-70 pipeline steel. The contrasting erosion mechanism on corroded carbon steel compared to pure erosion mechanism is instigated by the porous and brittle iron oxide products formed on the carbon steel surface after corrosion. The brittle nature of these oxide products makes the specimen vulnerable to erosion attack under subsequent aluminum oxide particle impacts. As a result, increase in erosion rates is observed, caused and enhanced by metal cuts and platelet fractures on the corroded surface.

4. CONCLUSIONS

Experiments were carried out to investigate the corrosion enhanced erosion behavior of carbon steel AISI 1020. Specimens were immersed in corrosive solution for 12h, 24 h, 36 h, 48 h, and 60 h. Specimens immersed for 24 h and 48 h were then subjected to erosion at six different impact angles

15°, 30°, 45°, 60°, 75° and 90°, using two different impact velocities (30 m/s and 60 m/s) at each impact angle. Based on the obtained results, the following conclusions can be drawn:

1. Immersion of carbon steel AISI 1020 led to the formation of loosely adherent brittle corrosion products which altered the surface conditions (roughness and hardness).
2. Significant increase in erosion rate was observed for 24 h immersed carbon steel 1020 which is attributed to the increased surface roughness and surface hardness after 24 h immersion in ferric chloride solution.
3. The variation in erosion rates of the corroded specimens was directly corresponding to the variation in surface roughness and hardness of the specimens. This indicates that the surface conditions play a major role in corrosion-enhanced erosion of carbon steel AISI 1020.
4. An increase in erosion rate with increase in impact velocity was observed. This is attributed to the increase in particle kinetic energy with an increase in particle impact velocity resulting in higher shear stresses which causes more mass loss.
5. SEM revealed evidence of material cutting, shredding and localized fractures in eroded-corroded AISI 1020.

ACKNOWLEDGEMENTS
The authors would like to acknowledge the support received from King Abdulaziz City for Science and Technology (KACST) for funding this work under the National Science Technology Plan (NSTIP) grant No. 11-ADV1619-04. Also, the support provided by the Deanship of Scientific Research (DSR) at King Fahd University of Petroleum & Minerals (KFUPM) is gratefully acknowledged

References

1. R. J. K. Wood, 6.09 – Erosion/Corrosion, *Compr. Struct. Integr*. (2007) 395.
2. M. Matsumura, *Corros. Rev*., 12 (1994) 321.
3. A. Neville, T. Hodgkiess, and H. Xu, *Wear,* 233–235 (1999) 523.
4. R. C. Barik, J. A. Wharton, R. J. K. Wood, K. S. Tan, K. R. Stokes, and M. Planck, *Wear* 259 (2005) 230.
5. E. J. Wright, K. D. Efrid, J. A. Boros, and T. G. Hailey, *Nace Conference and Expo* (2008) 08629.
6. J. Maciel and S. M. L. Agostinho, *J. Appl. Electrochem*., 30 (2000) 981.
7. H. X. Guo, B. T. Lu, and J. L. Luo, *Electrochim. Acta*, 51 (2005) 315.
8. P. Novak and A. Macenauer, *Corros. Sci.*, 35 (1993) 635.
9. T. Hong and W. Jepson, *Corros. Sci.*, 43 (2001) 1839.
10. K. P. Roberts, S. A. Shirazi, J. R. Shadley, E. F. Rybicki, and C. Joia, *Corros. Eng*., 68 (2012) 1.
11. R. O. Rihan and S. Nešić, *Corros. Sci.*, 48 (2006) 2633.
12. R. Malka, S. Nesic, and D. A. Gulino, *Nace Conference and Expo*, (2006) 06594.
13. M. H. Koike, *J. Nucl. Mater.*, 342 (2005) 125.
14. K. Sasaki and G. Burstein, *Corros. Sc*i., 49 (2007) 92.
15. A. Neville, M. Reyes, and H. Xu, *Tribol. Int*., 35 (2002) 643.
16. M. Matsumura, Y. Oka, H. Hiura, and M. Yano, *ISIJ Int.*, 31 (1991) 168.
17. S. Aribo, R. Barker, X. Hu, and A. Neville, *Wear*, 302 (2013) 1602.
18. E. Hussain and M. Robinson, *Corros. Sci*.,49 (2007) 1737.
19. M. Aminul Islam, Z. N. Farhat, E. M. Ahmed, and A. Alfantazi, *Wear*, 302 (2013) 1592.
20. C. F. Dong, K. Xiao, X. G. Li, and Y. F. Cheng, *Wear*, 270 (2010) 39.
21. A. Neville and X. Hu, *Wear*,251 (2001) 1284.

22. J. C. Nava, F. Stott, and M. Stack, *Corros. Sci*., 35 (1993) 1045
23. ASTM G 31-72, Standard Practice for Laboratory Immersion Corrosion Testing of Metals, 1999.
24. ASTM G 119 - 04, Standard guide for determining synergism between wear and corrosion, ASTM Standards, 93 (2004) 1.
25. ASTM standard, G76-95, Standard practice for conducting erosion tests by solid particle impingement using gas jets, ASTM Standards., 95 (200) 1.
26. A. Ruff and L. Ives, *Wear*, 36 (1975) 195.
27. P. H. Shipway and I. M. Hutchings, *Wear,* 174 (1994) 169.
28. C. Gomes-Ferreira, D. Ciampini, and M. Papini, *Tribol. Int*., 37 (2004) 791.
29. K. E. García, A. L. Morales, C. A. Barrero, and J. M. Greneche, *Corros. Sci*., 48 (2006) 2813.
30. J. Hu, S. Cao, and J. Xie, *Anti-Corrosion Methods Mater.*, 60 (2013) 100.
31. K. C. Goretta and A. C. Thompson, *Mater. Sci. Eng*., 161 (1993) 7.
32. A. V Levy, Wear, 108 (1986) 1.
33. Y.-S. Choi and J.-G. Kim, *Corrosion,* 56 (2000) 1202.
34. T. Foley and A. Levy, *Wear,* 91 (1983) 45.
35. J. Malik, I. H. Toor, W. H. Ahmed, Z. M. Gasem, M. A. Habib, R. Ben-Mansour, and H. M. Badr, *J. Mater. Eng. Perform.*, 23 (2014) 2274.
36. S. A. Nelson, M. J. Baker, and W. F. Deans, Int. Pipeline Conference, (2004) 803.
37. A. Levy and M. Liebhard, *Wear*, 151 (1991) 381.
38. Y. I. Oka, H. Ohnogi, T. Hosokawa, and M. Matsumura, *Wear,* 203–204 (1997) 573.
39. C. T. Morrison, R. O. Scattergood, and J. L. Routbort, *Wear*, 111 (1986) 1.
40. G. L. Sheldon and I. Finnie, *J. Eng. Ind*., 88 (1965) 387.
41. L. E. K. Hein and P. G. Shewmon, *Wear,* 89 (1983) 291.
42. I. Finnie, *Wear*, 3 (1960) 76.
43. J. R. Laguna-Camacho, A. Marquina-Chávez, J. V. Méndez-Méndez, M. Vite-Torres, and E. A. Gallardo-Hernández, *Wear*, 301 (2013) 398.